



#### Available online at www.sciencedirect.com

### **ScienceDirect**

Proceedings
of the
Combustion
Institute

Proceedings of the Combustion Institute 38 (2021) 6631–6639

www.elsevier.com/locate/proci

# P-DRGEP: a novel methodology for the reduction of kinetics mechanisms for plasma-assisted combustion applications

Aurélie Bellemans <sup>a,b,c,1,\*</sup>, Nicholas Kincaid <sup>d,1</sup>, Nicholas Deak <sup>a</sup>, Perrine Pepiot <sup>d</sup>, Fabrizio Bisetti <sup>a</sup>

a Department of Aerospace Engineering and Engineering Mechanics, University of Texas at Austin, Austin, TX 78712, USA
 b Département d'Aéro-Thermo-Mécanique, Ecole Polytechnique de Bruxelles, Université Libre de Bruxelles, Bruxelles 1050,
 Belgium

<sup>c</sup> Combustion and Robust Optimization Group (BURN), Vrije Universiteit Brussel and Université Libre de Bruxelles, Bruxelles 1050, Belgium

<sup>d</sup> Sibley School of Mechanical and Aerospace Engineering, Cornell University, Ithaca, NY 14853, USA

Received 7 November 2019; accepted 28 June 2020 Available online 12 September 2020

#### **Abstract**

Detailed kinetics mechanisms for plasma-assisted combustion contain numerous species and reactions that model the interplay between non-equilibrium plasma processes and hydrocarbon oxidation. While physically accurate and comprehensive, such detailed mechanisms are impractical for simulations of unsteady multi-dimensional plasma discharges and their effect on reactive mixtures in practical devices. In this work, we develop and apply a novel methodology for the reduction of large detailed plasma-assisted combustion mechanisms to smaller skeletal ones. The methodology extends the Directed Relation Graph with Error Propagation (DRGEP) approach in order to consider the energy branching characteristics of plasma discharges during the reduction. Ensuring tight error tolerances on the relative proportions of energy lost by the electrons to the various classes of impact processes (i.e. vibrational and electronic excitation, ionization, and impact dissociation) is key to preserving the correct discharge physics in the skeletal mechanism. To this end, new targets that include energy transfers are defined and incorporated in DRGEP. The performance of the novel framework, called P-DRGEP, is assessed for the simulation of ethylene-air ignition by nanosecond repetitive pulsed discharges at conditions relevant to supersonic combustion and flame holding in scramjet cavities, i.e. from 600 K to 1000 K, 0.5 atm, and equivalence ratios between 0.75 and 1.5. P-DRGEP is found to be greatly superior to the traditional reduction approach applied to plasma-assisted ignition in that it generates a smaller skeletal mechanism with significantly lower errors. For ethylene-air ignition at the target conditions, P-DRGEP generates a skeletal mechanism with 54 species and 236 reactions, resulting in a 84% computational speed-up for ignition simulations, while guaranteeing errors below 10% on the time required

<sup>\*</sup> Corresponding author.

E-mail addresses: aurelie.bellemans@ulb.be, aurelie.bellemans@utexas.edu (A. Bellemans).

<sup>&</sup>lt;sup>1</sup> Co-first authors

for ignition following the first pulse, 1% on the mean electron energy, between 4 and 35% on electron energy losses depending on the process, and 5% on the laminar flame speed.

© 2020 The Combustion Institute. Published by Elsevier Inc. All rights reserved.

Keywords: Plasma-Assisted Combustion; DRGEP; Kinetics Reduction; Skeletal Chemistry; Ethylene Ignition

#### 1. Introduction

The use of repetitive non-thermal plasma discharges allows for the efficient ignition of fuel-air mixtures in difficult regimes through fast heating and the generation of reactive species such as radicals and excited atoms and molecules [1]. The discharge deposits energy in the internal degrees of freedom of the particles (e.g. vibrational and electronic states) through inelastic collisions with electrons. This energy deposition enhances the reactivity of the mixture and leads to more robust ignition and stable flames, a demonstrated by experimental evidence [2,3]. A comprehensive overview of the state of the art on plasma-assisted ignition and combustion is given in several review articles [4–6].

Detailed reaction kinetics mechanisms are crucial in modelling the effect of non-equilibrium plasma on combustion chemistry. Due to the large number of species in detailed mechanisms (e.g. hundreds of species and thousands of reactions), the computational cost of high-fidelity simulations remains a challenge despite advancements in computing power. A common strategy consists in reducing large mechanisms to a skeletal form by discarding unimportant species and reactions.

Graph-based reduction methods have been widely adopted for this purpose, with a large number of variants now available as stand-alone techniques or coupled with adaptive methodologies [7–13]. In these techniques, the chemical kinetics network is turned into a directed graph, each node representing a species. Weighted edges are placed between nodes if the corresponding species interact directly with one another through elementary reactions. Skeletal mechanisms are obtained through the elimination of unimportant graph edges and nodes. The techniques vary based on the definition of the edges' weights and the graph search procedure used to identify unimportant branches. In this work, we focus on the DRG with Error Propagation (DRGEP) variant [14]. In contrast to other graph-based techniques, DRGEP allows the user to directly specify input targets whose dynamics are to be captured accurately. The elimination process is refined by evaluating the influence of any specie or reaction on the target of interest, typically a fuel or a product, by propagating local influences throughout the graph. An extensive literature documents the advantages and successes of the DRG and DRGEP methods [15–18].

Plasma-assisted combustion comes with kinetic pathways and dynamic behaviors not observed in conventional combustion, and it is currently unclear how the energy-exchange processes pertaining to non-equilibrium electrons steer the reduction procedure and affect the selection of species to be removed. This work explores the limitations of conventional reduction tools when applied to plasma-assisted combustion mechanisms, and proposes a plasma-specific extension to the DRGEP method (P-DRGEP). The novelty lies in the formulation of plasma-specific targets to enable a much finer discrimination between important and unimportant plasma and conventional combustion species and reactions. The predictive capability of the resulting skeletal mechanism is assessed by considering the energy branching of the plasma discharge, peak mean electron energy, and equilibrium temperature and composition after ignition. This comprehensive framework ensures that a physically accurate representation of key plasma processes is retained during reduction. The method is used to develop a skeletal mechanism for plasma-assisted ignition of low pressure ethyleneair mixtures at conditions relevant to supersonic combustion.

#### 2. Reactor model and ignition test cases

The governing equations describe the time evolution of a mixture in a closed isochoric and adiabatic reactor. The system of particles is described by two temperatures [19]:  $T_e$  for the electrons and T for all other particles (species). Let  $c_e$  indicate the concentration of electrons and  $c_i$  the concentration of particles other than electrons  $(i \neq e)$ .  $c_e$  and  $c_i$ evolve according to the following ordinary differential equations,

$$\frac{dc_e}{dt} = \omega_e, \qquad \frac{dc_i}{dt} = \omega_i. \qquad i \neq e$$
 (1)

 $\omega_e$  and  $\omega_i$  are the molar production rate of electrons and species i, respectively.  $u_e = u_e(T_e)$  and  $u_i = u_i(T)$  are the molar internal energy of the electrons and species i. The internal energy densities are  $U_e = u_e c_e$  for the electrons and  $U_i = u_i c_i$  for all other particles.  $c_{vi}$  is the specific heat at constant volume of species i and  $c_{ve} = 3k_B/2$  for the electrons ( $k_B$  is the Boltzmann constant). The evolution equations for T and  $T_e$  are

$$\sum_{i\neq e} c_{vi}c_i \frac{dT}{dt} = -\sum_{i\neq e} \omega_i u_i - Q_{el} - Q_{ix} - Q_l,$$

$$c_{ve}c_e \frac{dT_e}{dt} = -\omega_e u_e + Q_{el} + Q_{ix} + Q_l + Q_E. \quad (2)$$

 $Q_l$  describes the energy lost by the electrons through recombination processes,

$$Q_l = \sum_{k \in K} -u_e N_A q_k,\tag{3}$$

where K is the set of recombination reactions,  $q_k$  the rate coefficient for reaction k,  $u_e$  the internal energy of the electrons, and  $N_A$  the Avogadro number.  $Q_{ix}$  is the inelastic energy lost by the electrons due to ionization, dissociation and excitation processes,

$$Q_{ix} = \sum_{\ell \in I} -E_{exc,\ell} N_A q_\ell, \tag{4}$$

where L is the set of reactions involved, and  $E_{exc,\ell}$  is the excitation or ionization energy.  $Q_{el}$  describes the elastic energy exchanges,

$$Q_{el} = 3k_B \left( \sum_{i \in S, i \neq e} v_i^{el} m_e / m_i \right) n_e (T_e - T).$$
 (5)

 $m_i$  and  $m_e$  are the masses of species i and the electron,  $v_i^{el}$  is the elastic collision frequency between species i and the electron. The power deposited by the discharge per unit volume,  $Q_E$ , is modeled as a Gaussian pulse,

$$Q_E(t) = \frac{E}{\sigma\sqrt{2\pi}} \exp\left(-\frac{1}{2} \frac{(t-\mu)^2}{\sigma^2}\right),\tag{6}$$

with  $\mu$  the time of peak power,  $\sigma$  the pulse width related to the full-width-half-max FWHM =  $2\sqrt{2\ln 2\sigma}\approx 2.355\sigma$ , and E the energy density of the pulse. The discharge consists of a sequence of pulses with a pulse frequency f. These parameters are chosen in accordance with experiments to result in an ignition within 10 to 100  $\mu$ s of the first pulse [20]. Eqs. (1) and (2) are integrated with the stiff solver CVODE [21] in an in-house computer program (PACMAN) that uses the CHEMKIN library [22] for evaluation of thermodynamic properties and reaction rate coefficients.

Plasma-assisted ignition simulations are performed using a detailed kinetic mechanism with 163 species and 1167 reactions [23,24]. The ignition of an ethylene-air mixture is achieved by depositing energy in the form of a burst of pulses, as shown in Fig. 1. A sampling rate of 10 ns captures changes in chemistry between the pulses. During the discharge, the sampling time is reduced to 0.1 ns to capture the fast changes in plasma chemistry.

During each discharge, the electron reaches peak mean energies  $\approx 6.5$  eV, followed by rapid cooling. Energetic electrons form excited state particles, mostly of  $O_2$  and  $N_2$ , and the quenching reactions that follow excitation (e.g.  $N_2^* + O_2 \rightarrow N_2 \rightarrow N_2 + O_2 \rightarrow N_2 \rightarrow N_2 + O_2 \rightarrow N_2 \rightarrow$ 

Table 1 Configuration used for the ignition of ethylene-air mixtures using a burst of pulses

Temperature, $T_0$ [K]	600-1000
Pressure, $p_0$ [atm]	0.5
Equivalence ratio, $\phi$	0.75 - 1.5
Peak power density [kW/cm <sup>3</sup> ]	2000
FWHM [ns]	15
Pulse frequency, $f$ [kHz]	100
Number of pulses to ignition	4-8
Time to ignition, $\tau_{ig}$ [µs]	20-60

20) result in the formation of radicals as the excited particles thermalize. After a number of pulses, the concentration of carbon dioxide increases abruptly, signaling that conventional exothermic reactions responsible for most of the heat release rate undergo a rapid acceleration consistent with an ignition event. Thus, the instant in time when the rate of change in the number density of CO2 is maximum is taken to represent the time of ignition  $t^*$ . Then, the time to ignition is defined as  $\tau_{ig} = t^* - t_1$ , where  $t_1$  is the timing of the peak discharge power during the first pulse. Thus,  $\tau_{ig}$  represents the interval between the first pulse and ignition. The discharge parameters are chosen to guarantee ignition within  $\mathcal{O}(100 \,\mu\text{s})$  of the first pulse. The values of energy density per pulse employed in the study are comparable to those in experimental studies on plasma-assisted ignition and are reported in Tab. 1. The reactor is initialized with pressure  $p = p_0$ , temperature  $T = T_e = T_0$ , and a mixture of fuel and air with equivalence ratio  $\phi$ .  $T_0$  ranges from 600 K to 1000 K, while  $\phi$  ranges between 0.75 and 1.5.

Energy branching describes how much energy is lost by the electrons in ionization, excitation (electronic and vibrational), and impact dissociation processes. The electron impact reactions responsible for energy loss are arranged according to their class. The overall energy transfer, specific to each class, is defined as follows,

$$\Omega_i = \sum_{r \in \mathcal{R}_i} \Omega_r = \sum_{r \in \mathcal{R}_i} -E_{exc,r} N_A q_r, \tag{7}$$

where  $\mathcal{R}_i$  is the set of reactions belonging to class  $i = \{ion, ele, vib, dis\}$ . The classes are: ionization (e.g.  $e^- + O_2 \rightarrow O_2 + 2e^-$ ), vibrational excitation (e.g.  $e^- + N_2 \rightarrow N_2(v_1) + e^-$ ), electronic excitation (e.g.  $e^- + N_2 \rightarrow N_2(a^3\Sigma) + e^-$ ), and impact dissociation (e.g.  $e^- + O_2 \rightarrow O(^1D) + O + e^-$ ), respectively. Reactions producing electronically excited radicals from molecules following impact dissociation are grouped with dissociation reactions.

Figure 2 shows the relative energy lost by the electrons into the 4 classes of reactions after one pulse. Most of the energy is lost to electronic excitation. Energy loss to vibrational excitation shows a maximum after the pulse. Electronic excitation, dissociation, and ionization require higher electron energies (6 to 16 eV) than vibrational excitation

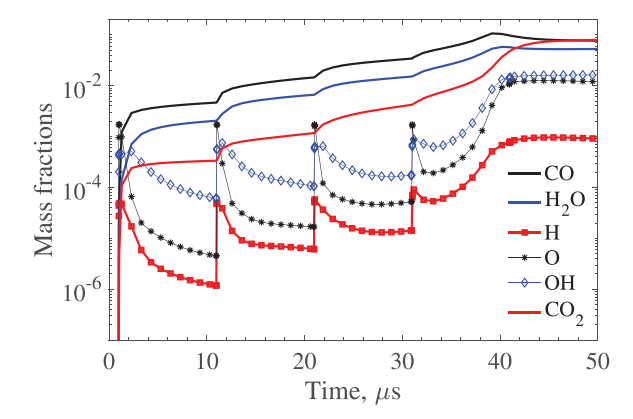


Fig. 1. A burst of pulses produces a sustained concentration of species and radicals for a stoichiometric C<sub>2</sub>H<sub>4</sub>-air mixture at 800 K and 0.5 atm. Ignition is achieved after 4 discharge pulses.

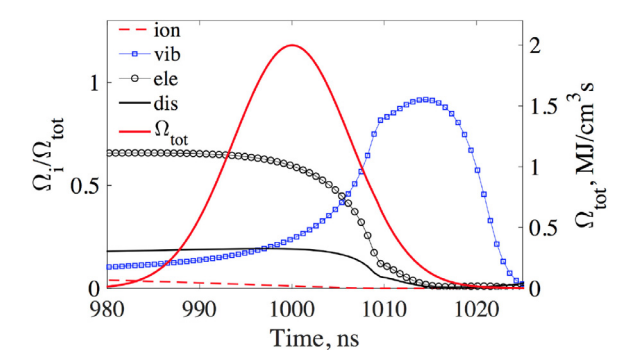


Fig. 2. Energy is deposited by the discharge (solid red line) and lost to ionization (dashed red line), electronic excitation (black line with circles), vibrational excitation (blue line with squares) and impact dissociation (thin black line).

(0.1 to 3 eV). Impact dissociation reactions are responsible for greater energy losses than ionization reactions.

#### 3. Plasma-targeted DRGEP

Graph-based techniques for chemical kinetic reduction use simulation data to quantify the coupling that exists between the species and reactions involved in a detailed mechanism, and identify those whose removal from the mechanism impacts the chemical model predictions minimally. The DRGEP method [14], more specifically, follows a 2-stage process: the coupling between species that interact with one another directly through elementary reactions is first quantified (*direct interactions*). Those direct interactions are then propagated to user-specified targets closely associated with a set of metrics, whose accurate prediction by the reduced mechanism is desired (*error propagation*). The outcome of this second stage is a global interaction coefficient  $R_{Ti}$  between any species or

reaction i in the mechanism and target T, which represents an a priori measure of the error that one would introduce in target T or its associated metric by removing species or reaction i. A library of increasingly reduced skeletal mechanisms is then generated by discarding species and reactions with the smallest values of the coefficients, and tested to identify the smallest mechanism that is able to predict the metrics of interest up to a specified error tolerance. A brief summary of the key steps and formulas involved is provided here, the reader being referred to [14] for more details.

The direct interaction coefficient  $r_{AB}$ , quantifying the direct influence of a species B on a species A, is defined as

$$r_{AB} = \frac{\left|\sum_{r \in \mathcal{R}} \nu_{r,A} q_r \delta_B^r\right|}{\max(P_A, C_A)},\tag{8}$$

where  $\mathcal{R}$  is the set of reactions in the detailed mechanism,  $\nu$  is the matrix of stoichiometric coefficients, and  $\mathbf{q}_r$  is the net rate of reaction r.  $\delta_B^r$  is equal to 1 if species B is present in the reaction (i.e. A and B both appear in reaction r), and 0 otherwise.  $P_A$  and

 $C_A$  are the total production and consumption rates of species A, respectively. The influence of species B on species A in the absence of a direct interaction via an elementary reaction is quantified using a path-dependent interaction coefficient. This coefficient is defined over a specific path p as the product of all the direct interaction coefficients between two directly interacting species  $S_j$  and  $S_{j+1}$ , along that path from B to A,

$$r_{AB,p} = \prod_{i=1}^{N_p} r_{S_j, S_{j+1}},\tag{9}$$

where  $N_p$  is the number of steps along the path, with  $S_1 = B$  and  $S_{N_p} = A$ . The global interaction coefficient between any species B and target T is defined finally as the coefficient of the most important path from species B to its target T,

$$R_{TB} = \max_{\forall p} r_{TB,p}. \tag{10}$$

The global interaction coefficient between a reaction and a target is defined similarly.

The most commonly used targets in conventional combustion applications include fuel, oxidizer, important combustion intermediates and products such as OH, CO, and CO<sub>2</sub>, and heat release rate. Although plasma-assisted combustion applications share the same objectives, e.g. the ignition and combustion of a fuel-air mixture, the kinetic pathways involved are quite different and specific to plasmas. Indeed, the discharge deposits energy into vibrational and electronic states of neutral species, and adds to the creation of chain-branching radicals such as O, H, and OH.

As we demonstrate later, using the standard combustion targets for the reduction of kinetic mechanisms for plasma-assisted combustion fails to recognize the importance of plasma-specific pathways, and yields skeletal mechanisms unable to capture the dynamics of plasma-assisted ignition. The issue as we diagnosed it, is that the intermediate species created by the non-equilibrium plasma, crucial for the energy branching, have low concentrations and very short life-time, and are therefore not coupled strongly with canonical combustion targets. Consequently, we propose a new implementation of the DRGEP methodology (P-DRGEP, for Plasma-DRGEP) that defines and incorporates new targets focused on energy branching. These plasma-specific targets guarantee that the plasma kinetics arising from the discharge are given equal consideration compared to traditional combustion kinetics, and are adequately retained in the skeletal mechanisms.

In contrast to conventional combustion, for which targets take the form of single, easily recognizable molecular species (e.g, CO, OH), energy branching is not characterized by a single species, and identifying *a priori* which species should be singled out and used as target to properly capture en-

ergy branching is not trivial. Instead, we propose to use the more comprehensive energy transfer variables,  $\Omega_i$ , as plasma-specific targets. This choice ensures that the key species for each type of energy transfer are automatically identified and retained by the DRGEP algorithm, bypassing entirely the need for manual selection by an expert user.

Accordingly, the direct interaction coefficient between any species B and the energy transfer variable  $\Omega_i$  is expressed as

$$r_{i,B} = \frac{\left| \sum_{r \in \mathcal{R}_i} \Omega_r \delta_B^r \right|}{|\Omega_i|},\tag{11}$$

where  $i = \{ion, vib, ele, dis\}$ . The global interaction coefficient between a energy transfer  $\Omega_i$  and any species B in the mechanism,  $R_{i,B}$ , is given by Eq. (10), with the variable  $\Omega_i$  now serving as end point for all paths considered in the error propagation.

#### 4. Results and discussion

#### 4.1. Reduction strategy

Because the importance of specific kinetic pathways depends on the local conditions, skeletal mechanisms are associated with a range of validity, implicitly determined by the set of thermochemical states used to calculate the interaction coefficients. Sampling thermo-chemical states in the parameter space  $(p, T, \phi)$  specific to the application is therefore crucial. Here, we follow standard sampling practices as documented in Ref. [14] whenever conventional combustion is considered, and adjust the collection of samples during plasma-assisted ignition to account for the discharge dynamics. Additional samples are retrieved during the discharge to capture the fast plasma chemistry ( $\Delta t_{sampling} =$ 0.1 ns), while fewer samples are collected between pulses ( $\Delta t_{sampling} = 10$  ns). Once the samples are available, the interaction coefficients, which determine the order in which the species and reactions are removed from the mechanism, are calculated by taking the maximum coefficient obtained from the set of targets as defined in Eqs. (10) and (11). A series of increasingly reduced skeletal mechanisms is generated by removing species and reactions progressively, those associated with the lowest coefficients being eliminated first.

An important feature of P-DRGEP is the metric-driven error control associated with the removal of species and reactions, allowing for a fast and reliable assessment of the accuracy of a given skeletal mechanism. A skeletal mechanism is deemed acceptable for a set of metrics and corresponding error tolerances if the relative error between the predictions of each metric with skeletal and detailed mechanisms falls below the user-defined error tolerance. In plasma-driven ignition,

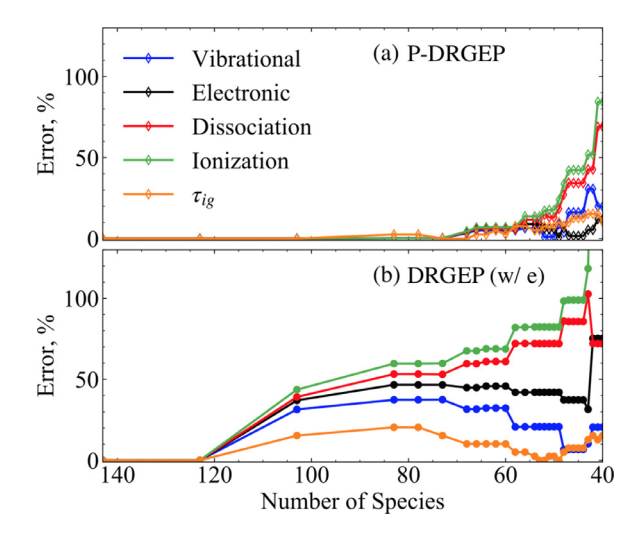


Fig. 3. P-DRGEP better controls the energy branching compared to DRGEP with the electron as an additional target for the reduction of ethylene-air at 800 K and  $\phi = 1$ .

 $\tau_{ig}$  is an important, but not sufficient metric, because of the significant role of the discharge in the timing process. In addition to  $\tau_{ig}$ , the following metrics are considered: post-ignition temperature and key radical mass fractions (O, H, and OH), and laminar flame speed. The laminar flame speed is considered given the importance of modeling flame propagation accurately following plasma-assisted ignition of reactive mixtures. Finally, in order to ensure that plasma physics are accurately represented in the skeletal mechanism, P-DRGEP uses energy branching as an additional metric through the definition of  $\theta_i$ , the integral of the energy transfer  $\Omega_i$  over the discharge pulses prior to ignition,

$$\theta_i = \int_{pulses} \Omega_i dt. \tag{12}$$

While not used as a metric, the peak mean electron energy,  $\epsilon_E$ , is also monitored during the reduction. Reduction is performed using ARCANE, a new python-based chemistry reduction code [25].

#### 4.2. Accurate energy branching with P-DRGEP

In this section, the performance of P-DRGEP in reducing the detailed 163 species chemical kinetics mechanism described in Section 3 to a skeletal one for plasma-assisted combustion is evaluated and discussed first for a single ignition case. The initial conditions are  $T_0 = 800$  K,  $p_0 = 0.5$  atm, and  $\phi = 1$ , and two species reduction approaches are considered and compared. The first approach uses DRGEP with a set of combustion targets (CO, CO<sub>2</sub>, C<sub>2</sub>H<sub>4</sub> and OH), supplemented by the electron. The second one uses P-DRGEP.

The error in  $\tau_{ig}$  and  $\theta_i$  as a function of the number of species retained in the skeletal mechanism

is shown in Fig. 3. A significant improvement on the energy branching predictions is observed using P-DRGEP (Fig. 3a), compared to canonical DRGEP, even with the electron as a target (Fig. 3b). For example, the error in  $\theta_i$  increases significantly ( $\geq 20\%$ ) for skeletal mechanisms smaller than 103 species, while P-DRGEP controls the error efficiently and up to  $\approx 50$  species.

Fig. 4, shows the energy branching for the two approaches at  $N_s = 53$ . The maximum error in  $\theta_i$  is  $\approx 15\%$  with P-DRGEP. The energy fluxes  $\Omega_i$  are shown for the first pulse, displaying clearly P-DRGEP's much improved agreement with the detailed mechanism relative to DRGEP.

To support our conclusions further, the mean electron energy is compared between the detailed and the skeletal mechanism with  $N_s = 53$  in Fig. 5. We note that not considering the electron as a target in DRGEP leads to  $\epsilon_E$  being overestimated by 25%, due to the early removal of  $N_2^+$ . Although adding the electron as a target in DRGEP brings the  $\epsilon_E$  error back to the same level as P-DRGEP, it fails at capturing the energy branching by the discharge as shown in Fig. 3. Moreover, this observation is an additional motivation for the using the P-DRGEP method as the manual selection of relevant species as targets based on expert knowledge fails at capturing the relevant plasma chemistry.

Table 2 compares the plasma species retained in the 53 species skeletal mechanism from DRGEP and P-DRGEP. A distinct improvement is observed using the novel approach as more key vibrational and electronically excited species are retained automatically with P-DRGEP: 7 key electronically excited states are retained compared to only 2 for DRGEP, which explains the inaccurate prediction of energy branching in Fig. 3.

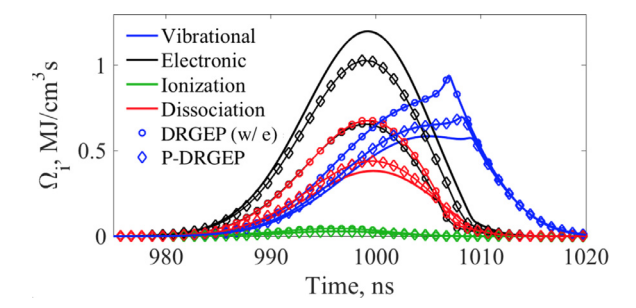


Fig. 4. The energy fluxes are compared for DRGEP (w/ e) and P-DRGEP at 800 K and  $\phi = 1$  for an example skeletal mechanism with  $N_s = 53$  species.

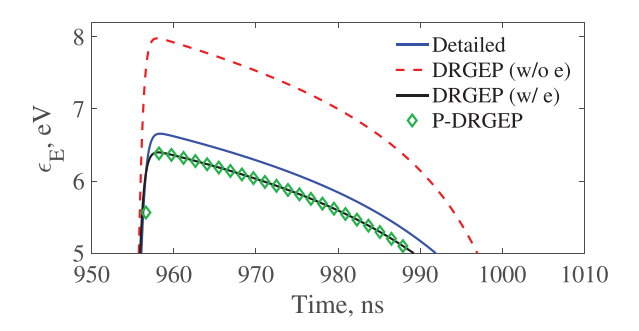


Fig. 5. The mean electron energy is compared for various targets at 800 K and  $\phi = 1$  for an example skeletal mechanism with  $N_s = 53$  species.

Table 2 Plasma species in skeletal mechanism  $N_s = 53$  for DRGEP (w/e) and P-DRGEP for ethylene-air ignition at 800 K and  $\phi = 1$ .

DRGEP (w/ e)	P-DRGEP
$N_2(v_1), N_2(v_2), N_2(v_3)$	$N_2(v_1), N_2(v_2), N_2(v_3)$
$N_2(v_4), N_2(v_5),$	$N_2(v_4), N_2(v_5), N_2(v_6),$
$N_2(a^3\Sigma)$ ,	$N_2(a^3\Sigma), N_2(w^3\Delta),$
	$N_2(c^3\Pi), N_2(b^3\Pi),$
$O(^{1}D), O_{2}(a^{1}\Delta), O_{2}(b^{1}\Sigma),$	$O(^{1}D)$ , $O_{2}(a^{1}\Delta)$ , $O_{2}(b^{1}\Sigma)$ ,
$N_2^+, O_2^+$	$N_2^+, O_2^+$

## 4.3. Comprehensive chemistry reduction for plasma-assisted ethylene-air combustion

We seek to generate a skeletal mechanism capable of reproducing the behavior of the detailed mechanism for plasma-assisted ignition of ethylene-air mixtures at  $600 \le T_0 \le 1000$  K and  $0.75 \le \phi \le 1.5$ . The P-DRGEP methodology is employed to this end.

Although our main focus lies on the ignition of the mixture, the skeletal mechanism must also be capable of simulating the propagation of a flame accurately. Therefore, the algorithm now considers thermo-chemical samples from both 0D ignition cases characterized above, and 1D unstretched freely propagating laminar premixed flames at 800 K, 0.5 atm, and equivalence ratios ranging from 0.75 to 1.5. The targets used for all 0D samples are

the same as above: CO, CO<sub>2</sub>, C<sub>2</sub>H<sub>4</sub>, OH, e, and the energy transfer variables  $\Omega_i$ . Only heat release is considered as target for the 1D samples.

To maximize the efficiency of the reduction procedure, we adopt an automatic multi-stage species and reaction reduction approach, in which both unimportant species and unimportant reactions are removed [14]. In contrast to the previous section, where the reduction was allowed to proceed regardless of the level of error introduced, we impose here specific error tolerances for the set of metrics of interest, and stop the reduction as soon as one of these tolerances is exceeded. The maximum error tolerances are 10% for  $\tau_{ig}$ , 40% for  $\theta_i$ , 2% for the equilibrium temperature (corresponding to a  $\approx$  60 K error), and 5% on the laminar flame speed,  $S_L$ .

With those constraints imposed, P-DRGEP generates a skeletal mechanism with 54 species and

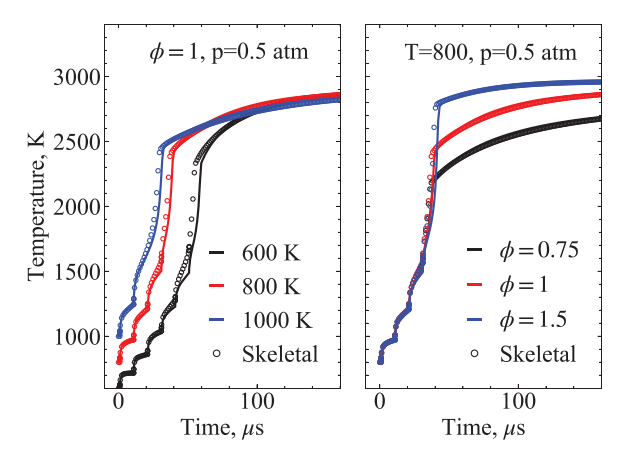


Fig. 6. Comparison of the gas temperature between the detailed and the skeletal mechanism with  $N_s = 54$ .

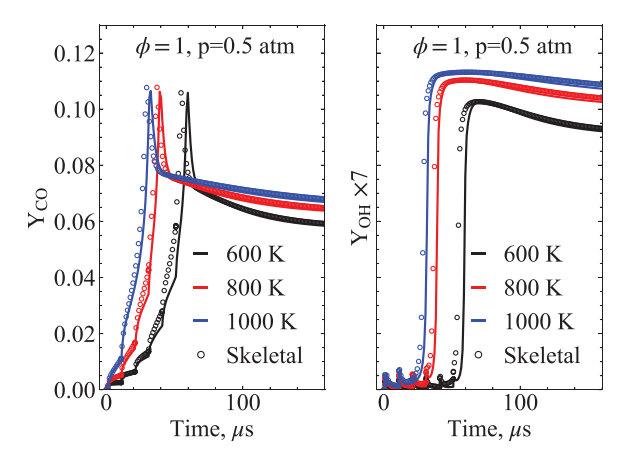


Fig. 7. Comparison of the species mass fractions between the detailed against the skeletal mechanism with  $N_s = 54$  for CO and OH.

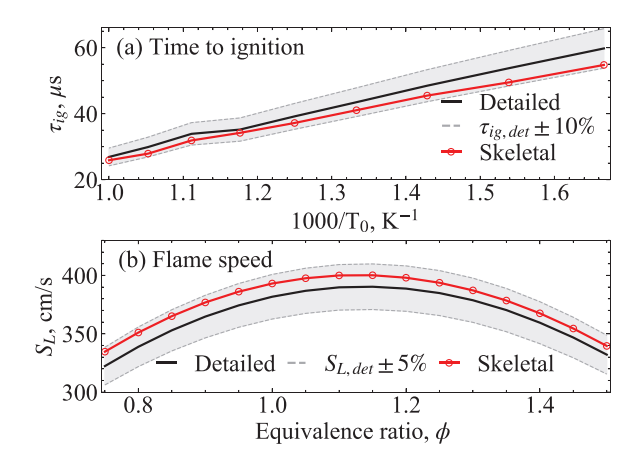


Fig. 8. Comparison of (a)  $\tau_{ig}$  (max. error 5%) and (b)  $S_L$  (max. error 5%) obtained with the detailed and the skeletal mechanism.

236 reactions, corresponding to a 67% reduction in the number of species, 80% reduction in the number of reactions, and a computational speed-up for the ignition simulations of 84%. The maximum error over all temperatures and equivalence ratios is  $\approx$  8% for  $\tau_{ig}$ , 35% for  $\theta_{ion}$ , 30% for  $\theta_{dis}$ , 8% for  $\theta_{ele}$ , and 4% for  $\theta_{vib}$ . Both the equilibrium temperature and the mean peak electron energy are reproduced with less than 1% error. The detailed and skeletal mechanism generated by P-DRGEP are available as supplementary material.

Excellent agreement is obtained for the gas temperature between the detailed and the skeletal mechanism for various  $T_0$  and  $\phi$ , as shown in Fig. 6. The species mass fractions of CO and OH are compared in Fig. 7. The equilibrium composition is retrieved accurately also. The time to ignition predicted by the detailed and the skeletal mechanisms is shown in Fig. 8a. The maximum error is found at the lowest temperatures (8% for  $T_0 = 600$  K). Figure 8b shows that the flame speed calculated with the skeletal mechanism stays within a 5% error of the detailed simulations in the range of equivalence ratios considered.

#### 5. Conclusions

A comprehensive reduction framework, P-DRGEP, is developed in order to reduce large kinetics mechanisms for plasma-assisted combustion into smaller skeletal ones. This novel methodology retains non-equilibrium plasma physics by upholding narrow error tolerances on the energy branching characteristics of the discharge. Starting from a detailed mechanism for ethylene-air with 163 species and 1167 reactions, P-DRGEP is used to develop a skeletal mechanism of 54 species and 236 reactions with errors below 10% on time to ignition, 1% on mean electron energy, between 4 and 35% on electron energy losses, depending on the process, and 5% on laminar flame speed. The skeletal mechanism is assessed for conditions relevant to supersonic combustion at 0.5 atm, temperatures of 600 to 1000 K, and equivalence ratios of 0.75 to 1.5. A computational speed-up greater than 80% is achieved, showing the potential of P-DRGEP to enable predictive multi-dimensional simulations of plasma-assisted combustion.

#### **Declaration of Competing Interest**

None.

#### Acknowledgments

A. Bellemans was supported by a fellowship of the B.A.E.F. and the F.R.S.-FNRS. N. Deak and F. Bisetti were sponsored in part by NSF Grant No. 190377 and DOE grant DE-EE0008874, P. Pepiot by NSF Grant No. 1653609. N. Kincaid was supported by NSF Grant No. DGE-1650441.

#### Supplementary material

Supplementary material associated with this article can be found, in the online version, at doi:10.1016/j.proci.2020.06.363.

#### References

- [1] Y. Ju, W. Sun, *Prog. Energ. Combust. Sci.* 48 (2015) 21–83.
- [2] M.S. Bak, H. Do, M.G. Mungal, M.A. Cappelli, Combust. Flame 159 (10) (2012) 3128–3137.
- [3] N. Tsolas, K. Togai, Z. Yin, K. Frederickson, R.A. Yetter, W.R. Lempert, I.V. Adamovich, *Combust. Flame* 165 (2016) 144–153.
- [4] A. Starikovskiy, N. Aleksandrov, Prog. Energ. Combust. Sci. 39 (1) (2013) 61–110.
- [5] I.V. Adamovich, W.R. Lempert, Plasma Phys. Control. Fusion 57 (1) (2014) 014001.
- [6] S. Starikovskaia, J. Appl. Phys. D. 47 (35) (2014) 353001.
- [7] A.B. Bendtsen, P. Glarborg, K. Dam-Johansen, Comput. Chem. 25 (2) (2001) 161–170.
- [8] T. Lu, C.K. Law, *Proc. Combust. Inst.* 30 (1) (2005)
- 1333–1341. [9] W. Sun, Z. Chen, X. Gou, Y. Ju, *Combust. Flame* 157
- (7) (2010) 1298–1307.[10] L. Tosatto, B.A.V. Bennett, M.D. Smooke, *Combust.*
- Flame 160 (9) (2013) 1572–1582.
- [11] A. Stagni, A. Frassoldati, A. Cuoci, T. Faravelli, E. Ranzi, Combust. Flame 163 (2016) 382–393.
- [12] Y. Liang, S.B. Pope, P. Pepiot, *Combust. Flame* 162 (2015) 3236–3253.
  [13] W. Sun, X. Gou, H.A. El-Asrag, Z. Chen, Y. Ju, *Com-*
- bust. Flame 162 (4) (2015) 1530–1539.
- [14] P. Pepiot-Desjardins, H. Pitsch, Combust. Theor. Model. 12 (6) (2008) 1089–1108.
- [15] K.E. Niemeyer, C. Sung, M.P. Raju, Combust. Flame 157 (9) (2010) 1760–1770.
- [16] Z. Li, M.T. Lewandowski, F. Contino, A. Parente, Energy Fuels 32 (10) (2018) 10121–10131.
- [17] Y. Chen, J. Chen, *Combust. Flame* 190 (2018) 293–301.
- [18] A. Felden, P. Pepiot, L. Esclapez, E. Riber, B. Cuenot, *Acta Astronaut*. 158 (2019) 444–459.
- [19] J.A. Bittencourt, Fundamentals of plasma physics, Springer Science & Business Media, 2013.
- [20] J.K. Lefkowitz, P. Guo, A. Rousso, Y. Ju, Phil. Trans. R. Soc. A 373 (2048) (2015) 20140333.
- [21] S.D. Cohen, A.C. Hindmarsh, P.F. Dubois, *Comput. Phys.* 10 (2) (1996) 138–143.
- [22] R. Kee, F. Rupley, J. Miller, Sandia Report SAND (1989) 89–8009.
- [23] I.V. Adamovich, T. Li, W.R. Lempert, *Phil. Trans. R. Soc. A* 373 (2048) (2015) 20140336.
- [24] N. Deak, A. Bellemans, F. Bisetti, Proc. Combust. Inst. 38 (2021).
- [25] 2019, (www.chemistry.cerfacs.fr/arcane).